Journal of the American Statistical Association

ISSN: 0162-1459 (Print) 1537-274X (Online) Journal homepage: www.tandfonline.com/journals/uasa20

Multi-Scale CUSUM Tests for Time Dependent Spherical Random Fields

Alessia Caponera, Domenico Marinucci & Anna Vidotto

To cite this article: Alessia Caponera, Domenico Marinucci & Anna Vidotto (16 Mar 2026): Multi-Scale CUSUM Tests for Time Dependent Spherical Random Fields, Journal of the American Statistical Association, DOI: 10.1080/01621459.2026.2639148

To link to this article: https://doi.org/10.1080/01621459.2026.2639148

Multi-Scale CUSUM Tests for Time Dependent Spherical Random Fields

Alessia Caponera*
Department of AI, Data and Decision Sciences, LUISS Guido Carli. Email: acaponera@luiss.it
and
Domenico Marinucci
Department of Mathematics, University of Rome Tor Vergata. Email: marinucc@mat.uniroma2.it
and
Anna Vidotto
Department of Basis and Applied Sciences for Engineering, Sapienza University of Rome. Email: anna.vidotto@uniroma1.it
*DM is grateful to the MUR Department of Excellence Programme *MatModToV* and to Mur *Grafia* for financial support. During the preparation of this work, AV was affiliated at the University of Naples Federico II and supported by the co-financing of the European Union - FSE-REACT-EU, PON Research and Innovation 2014-2020, DM 1062/2021. AC, DM and AV are members of INdAM/GNAMPA.

Abstract

This paper investigates the asymptotic behavior of structural break tests in the harmonic domain for time dependent spherical random fields. In particular, we prove a functional central limit theorem result for the fluctuations over time of the sample spherical harmonic coefficients, under the null of isotropy and stationarity; furthermore, we prove consistency of the corresponding CUSUM test, under a broad range of alternatives, including deterministic trend, abrupt change, and a nontrivial power alternative. Our results are then applied to NCEP data on global temperature: our estimates suggest that Climate Change does not simply affect global average temperatures, but also the nature of spatial fluctuations at different scales.

Keywords: Space-time processes, spherical Fourier analysis, non-stationarity, climate change

1 Introduction

The analysis of time dependent spherical random fields is the natural setting for a number of different areas of applications; some relevant examples include Cosmology, Geophysics and Atmospheric/Climate Sciences, see for instance [3, 4, 6, 20, 21] and the references therein for a small sample of recent contributions (more generally, spherical data have been recently considered in different frameworks by [5, 7–10], among others). In these areas, it is often a natural question to probe whether structural breaks have occurred over time; the most immediate example of such changes is obviously represented by shifts in the global mean (namely, averaged over space), which would correspond to Global Warming when studying temperature data. Such shifts can be investigated by means of a number of traditional statistical tools, such as the celebrated CUSUM test for structural breaks.

Our purpose in this paper is to exploit harmonic/spectral methods to investigate multi-scale structural breaks, i.e., modifications of the statistical model which may go beyond a simple global mean shift. A more rigorous and complete description of our environment will be given in the sections to follow; we believe, however, that it is useful to introduce from the start our motivations by means of a very preliminary analysis on a temperature data set.

In order to do so, let us first recall that a time dependent spherical random field is simply a collection of random variables $\{T(x,t), (x,t) \in \mathbb{S}^2 \times \mathbb{Z}\}$; under some regularity conditions (to be given below) the following spectral representation holds

$$T(x,t) = \sum_{\ell=0}^{\infty} T_\ell(x,t) = \sum_{\ell=0}^{\infty} \sum_{m=-\ell}^{\ell} \beta_{\ell m}(t) Y_{\ell m}(x) ,$$

where $\{Y_{\ell m}, m = -\ell, \ldots, \ell, \ell = 0,1,2,\ldots\}$ denotes the set of fully-normalized real spherical harmonics, an orthonormal basis for the space of square-integrable real-valued functions on the sphere, see [15]. Heuristically, each term $T_\ell(\cdot,t)$ can be viewed as the Fourier component of the spherical field at time *t* when projected onto basis elements characterized by fluctuations of typical scale $\theta_\ell \simeq \pi / \ell$. In particular, the Fourier coefficient corresponding to $\ell = 0$ is simply the sample mean at time *t* computed on the whole sphere, namely

$$\beta_{00}(t) = \frac{1}{\sqrt{4\pi}} \int_{\mathbb{S}^2} T(x,t) dx;$$

as such, it is for instance the typical statistic of interest when discussing global increments of the Earth temperature. As already mentioned, our aim in this paper is to explore possible changes occurring at different scales; for instance, it could be the case that even when the global mean is unaltered, or in addition to changes in the latter, other modifications occur in the fluctuations of the variable of interest.

This point is illustrated by a simple, very preliminary data analysis that we report here just as a motivating example; much greater details will be given below in Section 4. More precisely, we consider *global (land and ocean) surface temperature anomalies*; the dataset is built starting from the NCEP/NCAR monthly averages of the surface air temperature (in degrees Celsius) from 1948 to 2020, over a global grid with 2.5° spacing for latitude and longitude, see [13]. Following the World Meteorological Organization policy, temperature anomalies are obtained by subtracting the long-term monthly means relative to the 1981-2010 base period. They are then averaged over months to switch from a monthly scale to an annual scale (we refer also to the recent survey [23] for a general discussion on the role of Statistics for Climate Data; see also [16] and the references therein for some very recent contributions).

Figure 1 reports the observed temporal evolution of $\beta_{00}(t)$, which is nothing else than the sample spatial average of Earth temperature anomalies at time *t*; unsurprisingly, this global mean grows steadily from 1948 to 2020.

Let us now consider a plot of the fluctuations of the temperature, with respect to its historical mean (given in Figure 2). A careful inspection of the colors suggests that not only some regions exhibit greater changes than others (i.e., the Poles), but also that a small periodic pattern seems to appear, with greater fluctuations that are at an approximated distance of 40-60 degrees across different latitudes.

This point can be made clearer by introducing the spherical coordinates $\theta \in [0, \pi]$ (co-latitude) and $\phi \in [0, 2\pi)$ (longitude); in this coordinates, the spectral representation becomes

$$T(\theta, \phi; t) = \sum_{\ell=0}^{\infty} T_\ell(\theta, \phi; t) = \sum_{\ell=0}^{\infty} \sum_{m=-\ell}^{\ell} \beta_{\ell m}(t) Y_{\ell m}(\theta, \phi),$$

with the analytic expressions

$$Y_{\ell m}(\theta, \phi) = \begin{cases} \sqrt{\frac{2\ell+1}{2\pi}} \sqrt{\frac{(\ell - |m|)!}{(\ell + |m|)!}} P_{\ell |m|}(\cos\theta) \sin(|m|\phi) \text{for } m < 0 \\ \sqrt{\frac{2\ell+1}{4\pi}} P_{\ell 0}(\cos\theta) \text{for } m = 0 \\ \sqrt{\frac{2\ell+1}{2\pi}} \sqrt{\frac{(\ell - m)!}{(\ell + m)!}} P_{\ell m}(\cos\theta) \cos(m\phi) \text{for } m > 0 \end{cases},$$

$$P_{\ell m}(u) = \frac{1}{2^\ell \ell!} (1-u^2)^{m/2} \frac{d^{\ell+m}}{dt^{\ell+m}} (u^2 - 1)^\ell, \quad u \in [-1, 1], m \geq 0.$$

The $P_{\ell m}$'s are the well-known associated Legendre functions, whereas the $\beta_{\ell m}(t)$'s can be obtained by means of the Fourier transform

$$\int_{-\pi}^{\pi} \int_0^{2\pi} T_\ell(\theta, \phi; t) Y_{\ell m}(\theta, \phi) \sin\theta d\theta d\phi. \quad (1.1)$$

Note also that, for every $\ell = 0, 1, 2, \ldots,$ we have that

$$\int_{-\pi}^{\pi} T_\ell(\theta, \phi; t) d\phi = \sqrt{2\ell+1} \sqrt{\pi} \beta_{\ell 0}(t) P_{\ell 0}(\cos\theta) .$$

In other words, up to a deterministic function, each random process $\{\beta_{\ell 0}(t), t \in \mathbb{Z}\}$ captures the temporal evolution of the sample spatial mean for the spectral component corresponding to the multipole ℓ, computed at any given latitude. To explore their behavior, we plot in Figure 3 the observed evolution of $\beta_{\ell 0}(t)$ over the time span 1948-2020, for $\ell = 2, 4, 6, 8,$. It is remarkable that these coefficients appear indeed to grow over time, suggesting that further changes in the Earth temperature pattern may have occurred, in addition to the growth of the global average.

This preliminary data exploration suggests that even if we were to subtract the global temperature mean $\beta_{00}(t)$ from each time observation, in order to make it constantly equal to zero, the effects of Climate Change would still be visible in the form of structural changes on different scales. Our purpose in this paper is to devise a class of tests in order to investigate these phenomena more rigorously, which is what we start to do from the next section.

Remark 1 .

The harmonic/spectral methods used in the present paper can be easily extended to time dependent random fields defined over any two-point homogeneous space, such as for instance the d-dimensional hypersphere $\mathbb{S}^{d-1}$ embedded in $\mathbb{R}^d$. Nevertheless, given that our primary objective lies in exploring the potential applications of such a sphere-cross-time model within Cosmology, Geophysics, and Atmospheric/Climate Sciences, we deem it unnecessary to overload the notation and proofs of the main results with a degree of generality that extends beyond the intended scope and purpose of this work.

2 Model

In this section, we introduce our model of interest. In short, under the null we assume to deal with time dependent spherical random fields with a stationary (in time) but anisotropic (in space) mean function; on the other hand, we are going to probe alternatives that replace the stationary mean by introducing time-varying factors which may vary across the different multipole components. Moreover, the test statistic will be defined on a fixed window of consecutive frequencies (the so-called *multipoles* in the spherical setting), that is, on $\{\underline{\ell}, \underline{\ell}+1, \ldots, \overline{\ell}\}$, with $\underline{\ell}, \overline{\ell}$ being two fixed non-negative integer values such that $\underline{\ell} \leq \overline{\ell}$ and we define

$$\triangle_{\underline{\ell},\overline{\ell}} := \{(\ell, m) : \ell = \underline{\ell}, \ldots, \overline{\ell}, m = -\ell, \ldots, \ell\}.$$

From now on, we assume that all the constants involved in the *o*- and *O*-notations and in all upper and lower bounds depend on such multipole window $\{\underline{\ell}, \ldots, \overline{\ell}\}$.

2.1 The null hypothesis of stationarity

Let $\{Z(x,t), (x,t) \in \mathbb{S}^2 \times \mathbb{Z}\}$ denote a centered strictly isotropic (over space) and strictly stationary (over time) time dependent spherical random field, that is, a collection of random variables with finite variance and such that

$$\begin{aligned} Z(\cdot,\cdot) &\overset{d}{=} Z(g\cdot, \tau + \cdot) \qquad \tau \in \mathbb{Z}, \quad g \in SO(3), \\ \mathbb{E}[Z(x,t)] &= 0, \\ \mathbb{E}[Z(x_1,t_1)Z(x_2,t_2)] &=: \Gamma(\langle x_1, x_2 \rangle, t_2 - t_1), \end{aligned}$$

with $\langle \cdot, \cdot \rangle$ being the standard inner product in $\mathbb{R}^3$ and $SO(3)$ is the group of all rotations about the origin of $\mathbb{R}^3$ under the operation of composition. As anticipated above, it is well-known (see, e.g., [15]) that the space of square-integrable functions on the sphere admits as an orthonormal basis the fully-normalized spherical harmonics $\{Y_{\ell m}, m = -\ell, \ldots, \ell, \ell = 0,1,2,\ldots\}$, which are eigenfunctions of the spherical Laplacian and hence they satisfy the Helmholtz equation

$$\Delta_{\mathbb{S}^2} Y_{\ell m} = -\lambda_\ell Y_{\ell m}, \qquad \lambda_\ell = \ell(\ell+1), \qquad \ell = 1,2,\ldots,$$
$$\Delta_{\mathbb{S}^2} = \frac{1}{\sin\theta}\frac{\partial}{\partial\theta}\left(\sin\theta\frac{\partial}{\partial\theta}\right) + \frac{1}{\sin^2\theta}\frac{\partial^2}{\partial\phi^2}.$$

For fixed $t \in \mathbb{Z}$, the spectral representation theorem for isotropic random fields ensures that, in $L^2(\Omega \times \mathbb{S}^2)$,

$$Z(\theta,\phi;t) = \sum_{\ell=0}^{\infty}\sum_{m=-\ell}^{\ell} a_{\ell m}(t) Y_{\ell m}(\theta,\phi),$$

where the random coefficients $a_{\ell m}(t)$ are given by

$$a_{\ell m}(t) = \int_0^{\pi}\int_0^{2\pi} Z(\theta,\phi;t)\overline{Y_{\ell m}(\theta,\phi)}\sin\theta d\phi d\theta,$$

and are zero-mean and uncorrelated across ℓ and m.

The idea is now to consider a process $\{T(x,t), (x,t) \in \mathbb{S}^2 \times \mathbb{Z}\}$ that satisfies

$$T(x,t) - \mu(x) = Z(x,t), \quad (2.1)$$

for some deterministic $\mu(\cdot) \in L^2(\mathbb{S}^2)$. The anisotropic (but stationary) mean function then has the L^2-expansion

$$\mu(\theta,\phi) = \sum_{\ell=0}^{\infty}\sum_{m=-\ell}^{\ell} \mu_{\ell m} Y_{\ell m}(\theta,\phi),$$
$$\mu_{\ell m} = \int_{-\pi}^{\pi}\int_0^{2\pi} \mu(\theta,\phi) Y_{\ell m}(\theta,\phi)\sin\theta d\theta d\phi.$$

Hence, we can introduce our model under the null hypothesis in the next assumption.

Assumption 1 (Null hypothesis H_0).

Under the null hypothesis H_0, the field satisfies the equation in (2.1), and hence it has stationary mean function $\mathbb{E}[T(x,t)] = \mu(x)$ and spectral representation

$$T(x,t) = \sum_{\ell=0}^{\infty} \sum_{m=-\ell}^{\ell} a_{\ell m}(t) Y_{\ell m}(x) + \sum_{\ell=0}^{\infty} \sum_{m=-\ell}^{\ell} \mu_{\ell m} Y_{\ell m}(x) \ .$$

Under the assumptions on $\{Z(x,t), (x,t) \in \mathbb{S}^2 \times \mathbb{Z}\}$ we also have that the array of spherical harmonic coefficients $\{a_{\ell m}(t), m = -\ell, \ldots, \ell, \ell = 0,1,2,\ldots, t \in \mathbb{Z}\}$ is formed by zero-mean uncorrelated (over ℓ and m) and stationary (over t) processes, with covariances

$$C_\ell(\tau) := \mathbb{E}[a_{\ell m}(t+\tau) a_{\ell m}(t)] \ , \qquad t, \tau \in \mathbb{Z}.$$

Note that $\{C_\ell(0), \ell = 0,1,2,\ldots\}$ corresponds to the angular power spectrum of the spherical field at a given time point, for which we will simply write $\{C_\ell, \ell = 0,1,2,\ldots\}$; for simplicity and without loss of generality we assume that $C_\ell(0) > 0$ for all $\ell \in \{\underline{\ell}, \ldots, \overline{\ell}\}$. We also impose some regularity conditions on the behavior of higher-order cumulants, as detailed in the following subsection.

2.2 Cumulants and higher-order conditions

Let us first recall that the joint cumulant of a random vector $(X_1, \ldots, X_p)$ is just the Fourier coefficient in the expansion of the logarithm of the joint characteristic function (the expansion is implicitly assumed to exist), see [18]. Of course for Gaussian random variables cumulants of order strictly larger than 2 are exactly equal to zero; for random spherical harmonics coefficients of isotropic spherical processes, a number of further characterizations for their joint cumulants are discussed in [15, Chapter 6].

In this paper, we are allowing for general non-Gaussian behavior, imposing only the following very broad condition on the joint cumulants:

Assumption 2 .

For all integers $p \geq 2$ *and* $(\ell_j, m_j) \in \Delta_{\underline{\ell}, \overline{\ell}}$, $j = 1, \ldots, p$,

$$\sum_{\tau_1, \ldots, \tau_{p-1} = -\infty}^{+\infty} \left| \mathrm{cum}\left(a_{\ell_1, m_1}(t+\tau_1), \ldots, a_{\ell_{p-1}, m_{p-1}}(t+\tau_{p-1}), a_{\ell_p, m_p}(t)\right) \right| < +\infty. \quad (2.2)$$

Remark 2 .

Summability of the cumulants is a standard condition in asymptotic theory of stationary processes (see e.g. [17] and the references therein). For stationary time series it is fulfilled for instance by ARMA processes with i.i.d. innovations and finite moments of all orders. Likewise, by a careful exploitation of the diagram formula, see [15], subsection 4.3.1, it can be shown that it is fulfilled by polynomial transforms of Gaussian processes with summable covariances.

In view of the strict stationarity condition that we imposed above, the expression (2.2) is strictly invariant with respect to $t \in \mathbb{Z}$. In particular, condition (2.2) (for $p = 2$) implies the continuity of the spectral densities of the spherical harmonic coefficients; indeed, for any multipole ℓ, the associated spectral density function is well defined as

$$f_\ell(\lambda) := \frac{1}{2\pi} \sum_{\tau \in \mathbb{Z}} C_\ell(\tau) e^{-i\lambda\tau} , \qquad \lambda \in [-\pi, \pi] . \quad (2.3)$$

Assumption 3 .

For all integers $\ell \in \{\underline{\ell}, \ldots, \overline{\ell}\}$*, the spectral density at the origin is strictly positive, that is,* $f_\ell(0) > 0$.

This is a standard identifiability condition that is fulfilled, for instance, by all stationary invertible ARMA processes.

2.3 The test statistic

We start by defining some sample quantities that are needed in order to introduce our CUSUM test statistics, which can also be viewed as a form of Fourier domain testing for stationarity for functional valued time series, see [1, 12].

Definition 1 (Sample harmonic coefficients).

For $t = 1, 2, \ldots, N$*, the sample spherical harmonic coefficients are defined by*

$$\beta_{\ell m}(t) := \int_{\mathbb{S}^2} T(x,t) Y_{\ell m}(x) dx , \qquad (\ell, m) \in \Delta_{\underline{\ell}, \overline{\ell}}.$$

Note that we are implicitly assuming that the $\beta_{\ell m}(t)$'s can be estimated exactly from the observations, i.e., that the integrals defined in (1.1) can be computed without approximations. That is, we are adopting the assumption that the field is fully observed over the sphere so that it is possible to compute its Fourier coefficients, which is standard in the functional data analysis context.

Definition 2 (Sample harmonic averages).

The sample harmonic averages are defined as

$$\hat{\mu}_{\ell m} := \frac{1}{N} \sum_{t=1}^{N} \beta_{\ell m}(t) , \qquad (\ell, m) \in \Delta_{\underline{\ell}, \overline{\ell}}.$$

Definition 3 (Sample variance).

The sample variance is defined as

$$\hat{\sigma}^2 = \sum_{\ell=\underline{\ell}}^{\bar{\ell}} (2\ell+1) 2\pi \hat{f}_\ell(0), \quad \text{which estimates} \quad \sigma^2 := \sum_{\ell=\underline{\ell}}^{\bar{\ell}} (2\ell+1) 2\pi f_\ell(0),$$

where

$$2\pi \hat{f}_\ell(0) = \sum_{\tau=-k_N}^{k_N} \left(1 - \frac{|\tau|}{k_N+1}\right) \hat{C}_\ell(\tau) = \hat{C}_\ell(0) + 2\sum_{\tau=1}^{k_N} \left(1 - \frac{\tau}{k_N+1}\right) \hat{C}_\ell(\tau),$$

$$\hat{C}_\ell(\tau) = \frac{1}{2\ell+1} \frac{1}{N-|\tau|} \sum_{m=-\ell}^{\ell} \sum_{t=1}^{N-|\tau|} (\beta_{\ell m}(t) - \hat{\mu}_{\ell m})(\beta_{\ell m}(t+|\tau|) - \hat{\mu}_{\ell m}).$$

The bandwidth parameter k_N *is assumed to grow slower than* $\sqrt{N}$ *; formally,*

$$k_N \to \infty \quad \text{as} \quad N \to \infty \quad \text{and} \quad k_N = o\left(\sqrt{N}\right).$$

Definition 4 (The test statistic).

The CUSUM test statistic on which we shall focus is given by the following supremum

$$\sup_{s\in[0,1]} |A_N(s)| \quad (2.4)$$

with

$$A_N(s) := \begin{cases} \frac{1}{\sqrt{N}} \frac{1}{\hat{\sigma}} \% \sum_{t=1}^{[Ns]} \sum_{\ell=\underline{\ell}}^{\bar{\ell}} \% \sum_{m=-\ell}^{\ell} (\beta_{\ell m}(t) - \hat{\mu}_{\ell m}), & s \in [1/N, 1], \\ 0 & s \in [0, 1/N), \end{cases}$$

where $[\cdot]$ *denotes the floor function. In the following, when writing* $s \in [0,1]$ *we always implicitly make the previous distinction.*

As we shall see later, we will compute the critical values of the CUSUM test statistic (2.4) based on the limiting behavior of $\sup_{s\in[0,1]} |A_N(s)|$ as $N \to \infty$, see Theorem 1 (together with Remark 4) where it is shown that $A_N(\cdot)$ weakly converges to a Brownian Bridge. The distribution of the supremum of a Brownian Bridge is also called Kolmogorov-Smirnov distribution, and the derivation of its quantiles is standard (see, for instance, [14, Table 1]).

Remark 3 .

We recall, as mentioned right after Definition 1, that in the test statistic A_N we assume that we are observing the entire field $T(\cdot, t)$ over the sphere $\mathbb{S}^2$ at times $t = 1, \ldots, N$. This obviously

implies that we are able to compute the vector $\{\beta_{\ell m}(t), t = 1, \ldots, N\}$ (without approximation by assumption) and then to compute $A_N(s)$, $s \in [0,1]$.

2.4 The alternative hypothesis

We shall here introduce our model under the alternative; in this case, we allow the deterministic mean function to vary over time, and hence we consider a process $\{T(x,t), (x,t) \in \mathbb{S}^2 \times \mathbb{Z}\}$ that satisfies

$$T(x,t) - \mu(x,t) = Z(x,t), \quad (2.5)$$

for some $\mu(\cdot,t) \in L^2(\mathbb{S}^2)$, $t \in \mathbb{Z}$.

Assumption 4 (Alternative hypothesis H_1).

Under the alternative hypothesis H_1, the field satisfies the equation in (2.5), so that

$$T(x,t) = \sum_{\ell=0}^{\infty} \sum_{m=-\ell}^{\ell} a_{\ell m}(t) Y_{\ell m}(x) + \sum_{\ell=0}^{\infty} \sum_{m=-\ell}^{\ell} \mu_{\ell m}(t) Y_{\ell m}(x),$$

with

$$\mu_{\ell m}(t) = \mu_{\ell m;0} + N^{\alpha_\ell} g_{\ell m}\left(\frac{t}{N}\right), \qquad \alpha_\ell \in \mathbb{R}, t = 1, \ldots, N,$$

where $\mu_{\ell m;0} \in \mathbb{R}$ is an intercept value and $g_{\ell m}$ are bounded piecewise continuous functions on $[0,1]$. In addition, denoting with

$$\bar{\alpha} := \max_{\ell = \underline{\ell}, \ldots, \bar{\ell}} \alpha_\ell,$$

we assume that

$$\bar{\alpha} \geq -1/2, \quad \sum_{\ell \in \bar{\mathcal{I}}} \sum_{m=-\ell}^{\ell} \mathrm{Var}(g_{\ell m}(U)) \neq 0,$$

$\bar{\mathcal{I}}$ being the set of indexes $\{\ell \in \{\underline{\ell}, \ldots, \bar{\ell}\} : \alpha_\ell = \bar{\alpha}\}$ and $U \sim \mathrm{Unif}(0,1)$, and there exists $s \in (0,1)$ such that

$$\sum_{\ell \in \bar{\mathcal{I}}} \sum_{m=-\ell}^{\ell} \left(\int_0^s g_{\ell m}(t) dt - s \int_0^1 g_{\ell m}(u) du \right) \neq 0. \quad (2.6)$$

This model covers a number of nonparametric alternatives and allows to distinguish two possible regimes: *(I)* the *local alternative* regime, which occurs when $\bar{\alpha} = -1/2$, and *(II)* the *globally consistent* regime when $\bar{\alpha} > -1/2$. The first case will lead to a nontrivial power for the test, resulting from a mean shift of the asymptotic distribution of $A_N(s)$ compared to the one obtained under the null hypothesis H_0 (for a similar result in the linear regression setting, see for instance [19, Theorem 2]); as usual, the power of the test will depend on the size of the shift. In the second case we are going to obtain a consistency result for the test; specifically, the convergence to unity of the test power, with rates that depend on $\bar{\alpha}$ and k_N: see Theorem 2 together with the detailed discussion in Section 3.1.

3 Main Results

In this section, we state our main results, i.e., the asymptotic behavior of the test statistic under the null and alternative hypothesis. In the sequel, Assumptions 2 and 3 will be always taken to hold. To characterize the limiting distribution of our statistic of interest under the null, we recall a well-known definition.

Definition 5 .

A Brownian bridge is a zero-mean Gaussian process $W : [0,1] \to \mathbb{R}$ *with covariance function*

$$\mathbb{E}[W(s)W(s')] = (s \wedge s') - ss'.$$

Theorem 1 .

Under the null hypothesis H_0, *as* $N \to \infty$,

$$A_N(s) \Rightarrow W(s),$$

where $\Rightarrow$ *denotes as usual weak convergence in the Skorohod space* $D[0,1]$.

Remark 4 .

The previous result ensures the weak convergence under the null of our test statistic; threshold values for the excursion of Kolmogorov-Smirnov or Cramér-Von Mises statistics can hence be derived by analytic computations or simulations. Our next result studies the asymptotic behavior of the test statistic under H_1 in the two regimes anticipated in Section 2.4.

Theorem 2 .

Under the alternative hypothesis H_1, *as* $N \to \infty$, *we have*

(I) *if* $\bar{\alpha} = -1/2$,

$$A_N(s) \Rightarrow W(s) + \frac{1}{\sigma}\sum_{\ell\in\overline{\mathcal{I}}}\sum_{m=-\ell}^{\ell}\left(\int_0^s g_{\ell m}(t)dt - s\int_0^1 g_{\ell m}(u)du\right),$$

where $\overline{\mathcal{I}} = \{\ell \in \{\underline{\ell},\ldots,\overline{\ell}\} : \alpha_\ell = \bar{\alpha}\}$ *;*

(II) *if* $\bar{\alpha} > -1/2$, *there exists* $K > 0$ *such that, taking*

$$r_N(\bar{\alpha}) = \begin{cases} N^{\bar{\alpha}+1/2} & \text{when} \quad \bar{\alpha} \in (-1/2, 0) \quad \text{and} \quad k_N N^{2\bar{\alpha}} \to c \geq 0 \\ \sqrt{N/k_N} & \text{when} \quad \bar{\alpha} \in (-1/2, 0) \quad \text{and} \quad k_N N^{2\bar{\alpha}} \to +\infty \\ \sqrt{N/k_N} & \text{when} \quad \bar{\alpha} \geq 0 \end{cases},$$

we have that

$$\mathbb{P}\left(\sup_{s\in[0,1]} |A_N(s)| > K \cdot r_N(\bar{\alpha})\right) \to 1.$$

The proofs of Theorems 1 and 2 are given in Appendices B and C, respectively.

Remark 5 .

For case *(II)* in Theorem 2, as $N \to \infty$, we can take more explicitly

- $k_N = [N^\beta]$ *with* $0 < \beta < 1/2$, *and*

$$r_N(\bar{\alpha}) = \begin{cases} N^{\bar{\alpha}+1/2} & \text{if} \quad \bar{\alpha} \in (-1/2, -\beta/2] \\ N^{(1-\beta)/2} & \text{if} \quad \bar{\alpha} > -\beta/2 \end{cases};$$

- $k_N = [\log N]$, *and*

$$r_N(\bar{\alpha}) = \begin{cases} N^{\bar{\alpha}+1/2} & \text{if} \quad \bar{\alpha} \in (-1/2, 0) \\ \sqrt{N/\log N} & \text{if} \quad \bar{\alpha} \geq 0 \end{cases}.$$

Note that when $k_N = [N^\beta]$ with $0 < \beta < 1/2$, we have a phase transition for the rate of the power in $-\beta/2$, while when k_N grows logarithmically in N, the phase transition happens in 0. In the literature on CUSUM tests, a standard choice for k_N is $[N^{1/3}]$ – see, for instance, [22] and the references therein.

3.1 Three possible scenarios

In the following, we first analyze two possible specific models for the globally consistent regime, that is case *(II)* of Theorem 2, and then we study the power of the test in the case $\bar{\alpha} = -1/2$, that is the locally alternative regime, i.e., case *(I)* of Theorem 2.

We start by first recalling that, under Assumption 4,

$$\mu_{\ell m}(t) = \mu_{\ell m;0} + N^{\alpha_\ell} g_{\ell m}\left(\frac{t}{N}\right).$$

Deterministic trend.

In the first scenario we consider a growing algebraic trend (to the leading order) which can be different from multipole to multipole and can be assumed arbitrarily small:

$$\alpha_\ell > 0 \quad \forall \ell \in \{\underline{\ell}, \ldots, \bar{\ell}\} \quad \text{and} \quad g_{\ell m}(u) = \mu_{\ell m;1} u^{\alpha_\ell}.$$

This model can be even more generilzed by adding further power terms or oscillating components as a remainder, e.g.,

$$\mu_{\ell m}(t) = \mu_{\ell m;0} + \mu_{\ell m;1} t^{\alpha_\ell} + \mu_{\ell m;2}(t),$$

where $\mu_{\ell m;1}$ is a real coefficient and $\mu_{\ell m;2}(t)$ is a function in *t* such that

$$\lim_{t\to\infty} \frac{\mu_{\ell m;2}(t)}{t^{\alpha_\ell - \epsilon}} = 0, \text{ for some } \epsilon > 0;$$

these conditions are for instance satisfied when $\mu_{\ell m;2}(t) = t^{\alpha_\ell - \epsilon^*} \log t^\delta$, for some $\epsilon^* > 0$ and some $\delta \in \mathbb{R}$. In this scenario, we are in case *(II)* of Theorem 2 with $r_N(\bar{\alpha}) = \sqrt{N / k_N}$ and

$$K = \frac{s^\star \left|(s^\star)^{\bar{\alpha}} - 1\right| \sqrt{2\bar{\alpha}+1}}{2\bar{\alpha}} \frac{\left|\sum_{\ell\in\bar{\mathcal{I}}} \sum_{m=-\ell}^{\ell} \mu_{\ell m;1}\right|}{\left(\sum_{\ell\in\bar{\mathcal{I}}} \sum_{m=-\ell}^{\ell} \mu_{\ell m;1}^2\right)^{1/2}},$$

with $s^\star \in (0,1)$, see also Equation (C.1) in the proof of Theorem 2. Here, the set $\bar{\mathcal{I}}$ can be viewed as the collection of multipoles which exhibit the strongest non-linear trend; we are imposing that these multipoles have coefficients which do not sum to zero, i.e., $\sum_{\ell\in\bar{\mathcal{I}}} \sum_{m=-\ell}^{\ell} \mu_{\ell m;1} \neq 0$, otherwise the condition is clearly meaningless.

Abrupt change.

It is also natural to consider the following scenario, in which an abrupt change occurs at time location $[\eta N]$ with $\eta \in (0,1)$, that is,

$$\alpha_\ell = 0 \quad \forall \ell \in \{\underline{\ell}, \ldots, \bar{\ell}\} \quad \text{and} \quad g_{\ell m}(u) = \mu_{\ell m;1} \mathbf{1}_{\{u \geq \eta\}},$$

see e.g. [22]. This alternative can be generalized to model the presence of multiple change points; however, we stick to the *at most one change point* setting for simplicity. In this scenario, we are in case *(II)* of Theorem 2 with $r_N(\bar{\alpha}) = \sqrt{N / k_N}$ and

$$K = \frac{\left|(s^\star - \eta)\mathbf{1}_{\{s^\star \geq \eta\}} - s^\star(1-\eta)\right| \left|\sum_{\ell \in \bar{\mathcal{I}}} \sum_{m=-\ell}^{\ell} \mu_{\ell m;1}\right|}{2\sqrt{\eta(1-\eta)} \left(\sum_{\ell \in \bar{\mathcal{I}}} \sum_{m=-\ell}^{\ell} \mu_{\ell m;1}^2\right)^{1/2}}.$$

In particular, choosing $s^\star = \eta$,

$$K = \frac{\sqrt{\eta(1-\eta)}}{2} \frac{\left|\sum_{\ell \in \bar{\mathcal{I}}} \sum_{m=-\ell}^{\ell} \mu_{\ell m;1}\right|}{\left(\sum_{\ell \in \bar{\mathcal{I}}} \sum_{m=-\ell}^{\ell} \mu_{\ell m;1}^2\right)^{1/2}}.$$

Nontrivial power alternative.

Another interesting scenario is the one that yields nontrivial asymptotic power, which corresponds to case *(I)* of Theorem 2. In this case, denoting

$$\text{shift}(s) := \frac{1}{\sigma} \sum_{\ell \in \bar{\mathcal{I}}} \sum_{m=-\ell}^{\ell} \left(\int_0^s g_{\ell m}(t)dt - s \int_0^1 g_{\ell m}(u)du \right)$$

and with $q_{1-\gamma}$ the quantile of order $1-\gamma$ of $\sup_s |W(s)|$, the power of the test can be approximated, for *N* sufficiently large, by

$$\mathbb{P}\left(\sup_{s \in [0,1]} |W(s) + \text{shift}(s)| > q_{1-\gamma} \right) \geq \mathbb{P}(|W(s^\star) + \text{shift}(s^\star)| > q_{1-\gamma}) \quad (3.1)$$

$$= 1 - \mathbb{P}(-q_{1-\gamma} - \text{shift}(s^\star) < W(s^\star) < q_{1-\gamma} - \text{shift}(s^\star))$$
$$= 1 - \mathbb{P}(Z \in \left[\frac{-q_{1-\gamma} - \text{shift}(s^\star)}{\sqrt{s^\star(1-s^\star)}}, \frac{q_{1-\gamma} - \text{shift}(s^\star)}{\sqrt{s^\star(1-s^\star)}} \right]), \qquad (3.2)$$

for any choice of $s^\star \in (0,1)$. Note that the interval in (3.2) is of width $2q_{1-\gamma} / \sqrt{s^\star(1-s^\star)}$, which does not depend on the shift. Heuristically, whenever $\left|\text{shift}(s^\star)\right| \gg 1$, this interval is placed on the tails of a standard Gaussian random variable *Z*, and hence the probability in (3.1) is close to 1.

In the sections to follow, we illustrate the validity of these results by means of an extensive Monte Carlo study and an application to the NCEP temperature data.

4 Numerical Results and Applications to NCEP Data

In this section, we present some numerical evidence on the performance of the test under the null; we then explore the power of the procedure against different alternatives, and we finally implement our proposed methods on real data on global surface temperature anomalies.

4.1 Simulations under H_0

We generate *N* serially correlated Gaussian isotropic random fields on the sphere, through the simulations of their first *L* harmonic coefficients

$$\{a_{\ell m}(t),\ m = -\ell, \ldots, \ell,\ \ell = 0, \ldots, L-1,\ t = 1, \ldots, N\}.$$

Specifically, we simulate from the following stationary autoregressive model of order 1, independently over ℓ and *m*,

$$a_{\ell m}(t) \,|\, a_{\ell m}(t-1) \sim \mathcal{N}(\phi_\ell a_{\ell m}(t-1), (1-\phi_\ell^2) C_\ell(0)), \qquad a_{\ell m}(t) \sim \mathcal{N}\left(0, C_\ell(0)\right),$$

with autoregressive parameters

$$\phi_0 = 0.4, \quad \phi_1 = -0.3, \quad \phi_2 = 0.2, \quad \phi_3 = -0.1, \quad \phi_\ell = 10 \cdot \ell^{-3}, \text{ for } \ell = 4, \ldots, L-1.$$

and marginal variances

$$C_0(0) = \frac{2}{1-\phi_0^2}, \quad C_\ell(0) = \frac{2}{\ell(\ell+1)(1-\phi_\ell^2)}, \ \ell = 1, \ldots, L-1.$$

Our assumptions are easily seen to be satisfied in this case (see, for instance, [2, 4]). Note that the chosen model for $C_\ell(0)$ would not be acceptable for the full range of multipoles, because the resulting field would not have finite variance. However, this is not an issue here, as we are

considering only a finite range of values. If necessary, we can implicitly assume that, for greater ℓ values, the sequence decreases at a faster rate.

We then consider the following model

$$\beta_{\ell m}(t) = a_{\ell m}(t) + \mu_{\ell m},$$

with

$$\mu_{00} = 5, \quad \mu_{\ell 0} = -\frac{2}{\ell(\ell+1)} \text{ for } \ell \text{ even}, \quad \mu_{\ell m} = 0 \text{ otherwise.}$$

We fix $L = 20$, $k_N = [N^{1/3}]$, and we compute the test statistic on a equally-spaced grid on the unit interval where each bin is of length $1/N$, for $N = 50, 100, 200$. This is repeated, for each N, 2000 times in order to get the approximate distribution of the CUSUM test statistic $\sup_{s\in[0,1]} |A_N(s)|$, which is shown in Figure 4 for $N = 200$. Table 1 reports the approximate Type I error probability associated with the selected quantiles, which are $q_{0.90} = 1.22$, $q_{0.95} = 1.35$ and $q_{0.99} = 1.60$ (see, for instance, [14, Table 1]); it is immediately seen that these empirical error probabilities are extremely close to their nominal values, even for sample sizes of order $N = 50$.

4.2 Simulations under H_1

Let us now focus on the alternative hypothesis; under H_1, the mean depends on time, i.e.,

$$\beta_{\ell m}(t) = a_{\ell m}(t) + \mu_{\ell m}(t).$$

For the residuals we simulate from the same Gaussian autoregressive model used under H_0, while for the mean we consider the *deterministic trend* and *non trivial power alternative* scenarios presented in Section 3.1. For simplicity we set $\mu_{\ell m;0} = 0$ uniformly.

Again, all the results are obtained by fixing $k_N = [N^{1/3}]$ and computing the test statistic on a equally-spaced grid on the unit interval where each bin is of length $1/N$, for 2000 independent replicates.

Deterministic trend.

As a first model for the non-stationarity mean, we choose

$$\mu_{00}(t) = 5 \cdot t^{\alpha}, \quad \mu_{\ell 0}(t) = -\frac{2}{\ell(\ell+1)} \cdot t^{\alpha} \text{ for } \ell \text{ even}, \quad \mu_{\ell m}(t) = 0 \text{ otherwise,}$$

which corresponds to the *deterministic trend* scenario with a constant α over the multipoles' window, and coefficients

$$\mu_{00;1} = 5, \quad \mu_{\ell 0;1} = -\frac{2}{\ell(\ell+1)} \text{ for } \ell \text{ even}, \quad \mu_{\ell m;1} = 0 \text{ otherwise.}$$

In particular, we set $L = 10$, and we study the behaviour of the power as the number of temporal observations increases, for $\alpha = 0.2, 0.5, 1$. The approximate test's power obtained for different values of α is reported in Figures 5. The three different curves in each plot correspond to the three different quantiles respectively of order $1-\gamma = 0.90, 0.95, 0.99$. Of course for higher values of α the deterministic trends under the alternative are stronger and hence the probability of rejection under H_1 becomes very close to one even at rather small sample sizes. In any case the consistency of the testing procedures which was established by our theoretical results shows up clearly in the simulations, as demonstrated by the uniform convergence to unity of the rejection probabilities under all settings, as *N* diverges.

Nontrivial power alternative.

Finally we explore the boundary case alternative. More precisely, we consider the following model for the non-stationary mean

$$\mu_{00}(t) = 5 \cdot \frac{t^{\beta}}{N^{\beta+1/2}}, \quad \mu_{\ell 0}(t) = -\frac{c}{\ell(\ell+1)} \cdot \frac{t^{\beta}}{N^{\beta+1/2}} \text{ for } \ell \text{ even}, \quad \mu_{\ell m}(t) = 0 \text{ otherwise,}$$

for some $c, \beta > 0$, which corresponds to the *nontrivial power alternative* scenario with a constant $\alpha = -1/2$ over the mulitpoles' window, $g_{\ell m}(u) = u^{\beta}$, and coefficients

$$\mu_{00;1} = 5, \quad \mu_{\ell 0;1} = -\frac{2}{\ell(\ell+1)} \text{ for } \ell \text{ even}, \quad \mu_{\ell m;1} = 0 \text{ otherwise.}$$

Here, we set $L = 10$, $N = 100$, and $\beta = 1$, and we study the behaviour of the power as $\left| \sum_{\ell,m} \mu_{\ell m;1} \right|$ increases, which is obtained by increasing *c*. Indeed, we set $c = 2, 100, 200, 300, 400$. Figure 6 shows the results for the three different quantiles of order $1-\gamma = 0.90, 0.95, 0.99$.

Impact of bandwidth on the results.

As discussed earlier, choosing the bandwidth k_N is a crucial step, and a standard choice in the literature on CUSUM tests is $[N^{1/3}]$ – see, e.g., [22] and the references therein. In practice, with moderate sample sizes *N*, alternatives such as $[\log N]$ or $[N^{1/2}]$ yield comparable results (although, from a theoretical standpoint, they imply different asymptotics; see Theorem 2).

Nevertheless, the scale of k_N can influence the outcome. In our simulation study under H_1, for both the deterministic trend scenario with $\alpha = 0.2$ and the nontrivial power alternative, we increased the bandwidth to $k_N = 5 \cdot [N^{1/3}]$. In each case, this choice resulted in a decrease in power, as shown in Figure 7. This reduction is explained by the fact that a larger k_N increases the denominator of the test statistic, which shifts its distribution toward lower values.

4.3 Application to NCEP data

As mentioned in the Introduction, the above methodology is applied to *global (land and ocean) surface temperature anomalies*. More in detail, the dataset is built starting from the NCEP/NCAR monthly averages of the surface air temperature (in degrees Celsius) from 1948 to 2020 ($N = 73$), over a global grid with 2.5° spacing for latitude and longitude, see [13]. We recall that, following the World Meteorological Organization policy, temperature anomalies are obtained by subtracting the long-term monthly means relative to the 1981-2010 base period; they are then averaged over months to switch from a monthly scale to an annual scale.

Using the `HEALPix` package (see [11] and the official `HEALPix` website), we convert the gridded data into spherical maps with a resolution of $12 \cdot \text{NSIDE}^2$ pixels (NSIDE = 16) – see Figure 2. Then, we compute the Fourier coefficients and the test statistic based on the window of consecutive multipoles $\{0,1,\ldots,12\}$, and bandwidth $k_N = [N^{1/3}] = 4$.

The observed value of the CUSUM test statistic is about 3.27 (see also Figure 8), which strongly suggests rejecting the null hypothesis of a stationary (in time) mean function.

We now run the same test, neglecting the multipole $\ell = 0$, that is, subtracting at each time *t* the sample spatial average of the anomalies, which is then made constant over time. We then repeat the same approach, dropping in turn the first $\underline{\ell} - 1$ multipoles, for $\underline{\ell} = 2, 4, 6, 8$: this way we explore the existence of non-stationarity features that do not involve the mean or the following lowest multipoles. The values of the observed CUSUM test statistic are reported in Table 2, together with the associated approximate *p*-values, which are obtained from the supremum of 10^6 independent replicates of a Brownian bridge, each evaluated on a grid of 10^6 equally-spaced points over the unit interval – this is equivalent to approximate the so-called Kolmogorov-Smirnov distribution. Our test statistic is still significant at level $\gamma = 0.01$ in each of these cases, apart from the very last for which the approximate *p*-value is slightly higher (but still less than 0.05). These results strongly suggest that climate change occurs not only in the mean temperature at a global level but also in the nature of fluctuations on a number of different scales corresponding to a few dozen degrees. The meaning and consequences of these preliminary findings on the nature of non-stationarity for climate data are left for future investigations.

Conflict of Interest

The authors report there are no competing interests to declare.

References

[1] Alexander Aue and Anne van Delft. Testing for stationarity of functional time series in the frequency domain. *Ann. Statist.*, 48(5):2505–2547, 2020.

[2] Alessia Caponera. SPHARMA approximations for stationary functional time series on the sphere. *Stat. Inference Stoch. Process.*, 24(3):609–634, 2021.

[3] Alessia Caponera, Julien Fageot, Matthieu Simeoni, and Victor M. Panaretos. Functional estimation of anisotropic covariance and autocovariance operators on the sphere. *Electron. J. Stat.*, 16(2):5080–5148, 2022.

[4] Alessia Caponera and Domenico Marinucci. Asymptotics for spherical functional autoregressions. *Ann. Statist.*, 49(1):346–369, 2021.

[5] Dan Cheng, Valentina Cammarota, Yabebal Fantaye, Domenico Marinucci, and Armin Schwartzman. Multiple testing of local maxima for detection of peaks on the (celestial) sphere. *Bernoulli*, 26(1):31–60, 2020.

[6] Jorge Clarke De la Cerda, Alfredo Alegría, and Emilio Porcu. Regularity properties and simulations of Gaussian random fields on the sphere cross time. *Electron. J. Stat.*, 12(1):399–426, 2018.

[7] Marco Di Marzio, Agnese Panzera, and Charles C. Taylor. Nonparametric regression for spherical data. *J. Amer. Statist. Assoc.*, 109(506):748–763, 2014.

[8] Marco Di Marzio, Agnese Panzera, and Charles C. Taylor. Nonparametric rotations for sphere-sphere regression. *J. Amer. Statist. Assoc.*, 114(525):466–476, 2019.

[9] Minjie Fan, Debashis Paul, Thomas C. M. Lee, and Tomoko Matsuo. Modeling tangential vector fields on a sphere. *J. Amer. Statist. Assoc.*, 113(524):1625–1636, 2018.

[10] Minjie Fan, Debashis Paul, Thomas C. M. Lee, and Tomoko Matsuo. A multi-resolution model for non-Gaussian random fields on a sphere with application to ionospheric electrostatic potentials. *Ann. Appl. Stat.*, 12(1):459–489, 2018.

[11] Krisztof. M. Górski, Eric Hivon, Anthony. J. Banday, Benjamin. D. Wandelt, Frode. K. Hansen, Martin Reinecke, and Matthias Bartelmann. HEALPix: A Framework for High-Resolution Discretization and Fast Analysis of Data Distributed on the Sphere. *Astrop. J.*, 622(2):759–771, April 2005.

[12] Siegfried Hörmann, Piotr Kokoszka, and Gilles Nisol. Testing for periodicity in functional time series. *Ann. Statist.*, 46(6A):2960–2984, 2018.

[13] Eugenia Kalnay, Masao Kanamitsu, Robert Kistler, William Collins, Dennis Deaven, Lev Gandin, Y Zhu, et al. The NCEP/NCAR 40-year reanalysis project. *Bull. Am. Meteo. Soc.*, 77(3):437–472, 1996.

[14] Sangyeol Lee, Jeongcheol Ha, Okyoung Na, and Seongryong Na. The cusum test for parameter change in time series models. *Scand. J. Stat.*, 30(4):781–796, 2003.

[15] Domenico Marinucci and Giovanni Peccati. *Random Fields on the Sphere: Representation, Limit Theorems and Cosmological Applications*, volume 389 of *London Mathematical Society Lecture Note Series*. Cambridge University Press, 2011.

[16] Diana P. Ovalle-Muñoz and M. Dolores Ruiz-Medina. Climate change analysis from LRD manifold functional regression. *Stoch. Environ. Res. Risk Assess.*, 39:1555–1580, 2025.

[17] Victor M. Panaretos and Shahin Tavakoli. Fourier analysis of stationary time series in function space. *Ann. Statist.*, 41(2):568–603, 2013.

[18] Giovanni Peccati and Murad S. Taqqu. *Wiener Chaos: Moments, Cumulants and Diagrams*, volume 1 of *Bocconi & Springer Series*. Springer Milano, 2011.

[19] Werner Ploberger and Walter Krämer. The local power of the cusum and cusum of squares tests. *Econom. Theory*, 6(3):335–347, 1990.

[20] Emilio Porcu, Alfredo Alegria, and Reinhard Furrer. Modelling temporally evolving and spatially globally dependent data. *Int. Stat. Rev.*, 86(2):344–377, 2018.

[21] Emilio Porcu, Moreno Bevilacqua, and Marc G. Genton. Spatio-temporal covariance and cross-covariance functions of the great circle distance on a sphere. *J. Amer. Statist. Assoc.*, 111(514):888–898, 2016.

[22] Michael Robbins, Colin Gallagher, Robert Lund, and Alexander Aue. Mean shift testing in correlated data. *J. Time Ser. Anal.*, 32(5):498–511, 2011.

[23] Michael L. Stein. Some statistical issues in climate science. *Statist. Sci.*, 35(1):31–41, 2020.

Figure 1: *Global surface temperature anomalies data*: observed temporal evolution (annual scale) of $\beta_{00}(t)$ from 1948 to 2020.

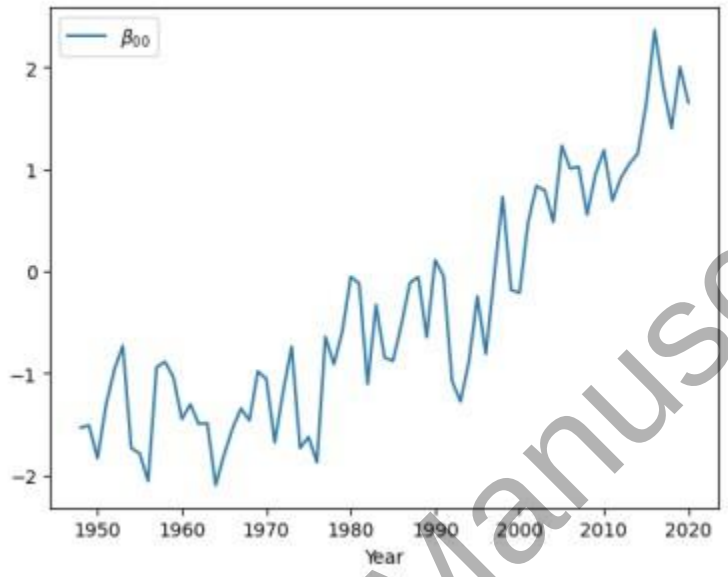

Figure 2: *Global surface temperature anomalies data*: global surface temperature anomalies (resolution: 3072 pixels) in years 1960, 1990, and 2020.

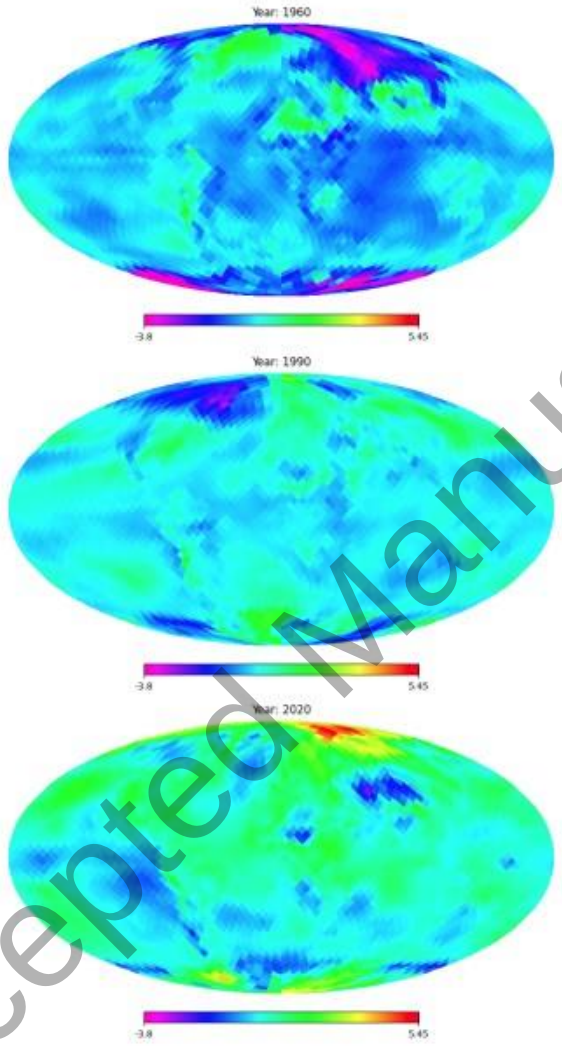

Figure 3: *Global surface temperature anomalies data*: observed temporal evolution (annual scale) of $\beta_{\ell 0}(t)$ from 1948 to 2020, for $\ell = 2, 4, 6, 8$.

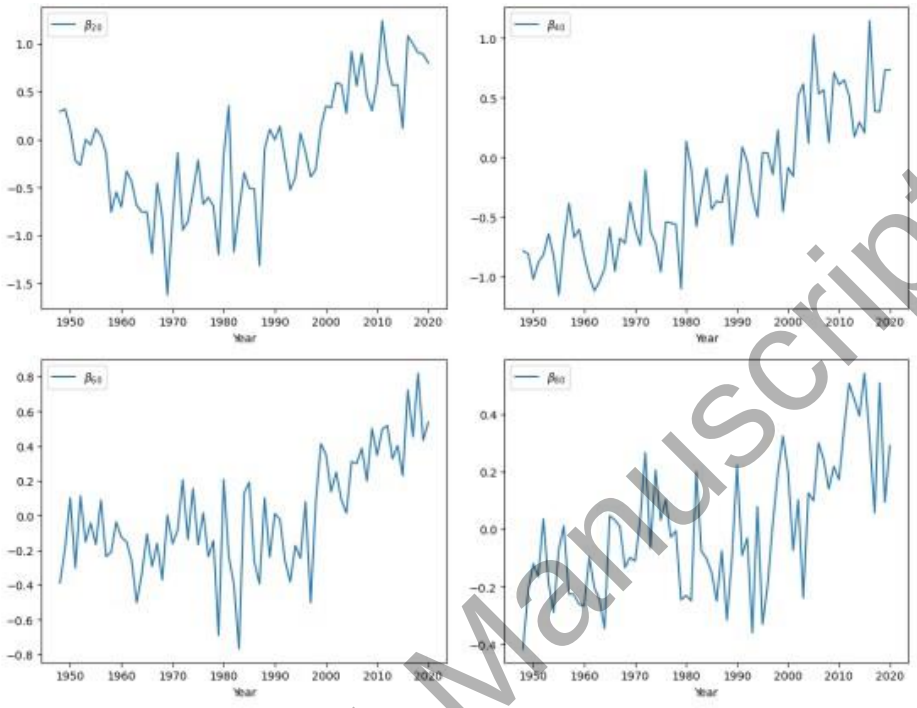

Figure 4: Histogram of the CUSUM test statistic (2.4) under H_0, computed for $L = 20$, $N = 200$, bandwidth $k_N = [N^{1/3}] = 5$, and based on 2000 independent replicates.

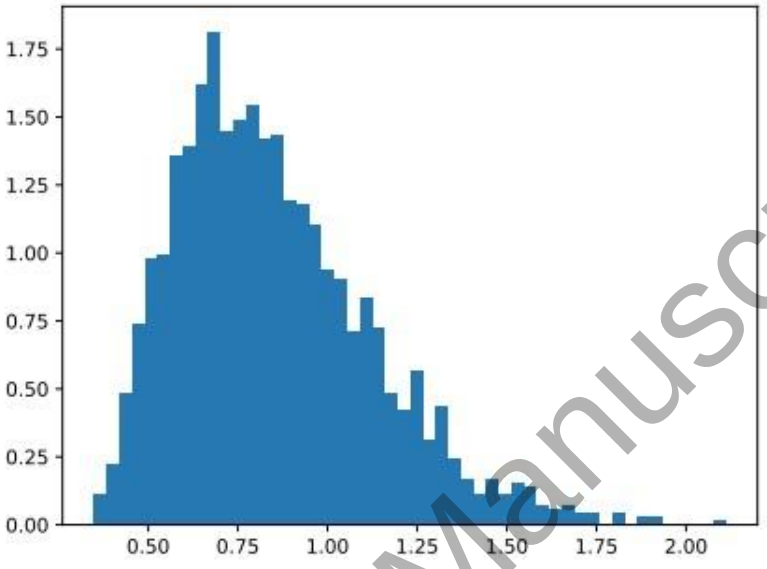

Figure 5: From top to bottom: test's power under the *deterministic trend* scenario for $\alpha = 0.2, 0.5, 1$, computed for $L = 10$, bandwidth $k_N = [N^{1/3}]$, and based on 2000 independent replicates. The lines correspond to the selected quantiles of order 0.90 (blu line), 0.95 (orange line), 0.99 (green line).

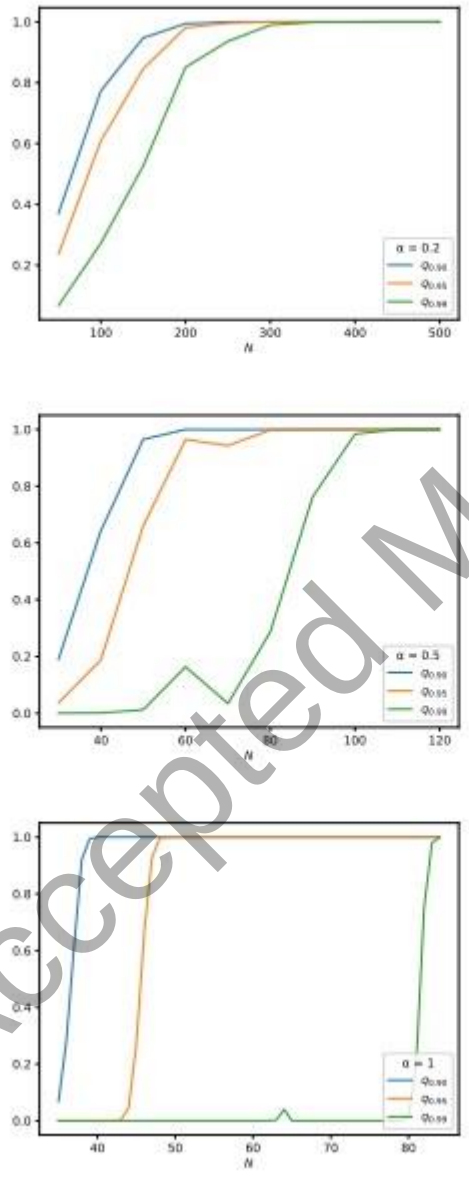

Figure 6: Test's power under the *nontrivial power alternative* scenario, computed for $L=10$, $N=100$, bandwidth $k_N=[N^{1/3}]=4$, and based on 2000 independent replicates. The lines correspond to the selected quantiles of order 0.90 (blu line), 0.95 (orange line), 0.99 (green line).

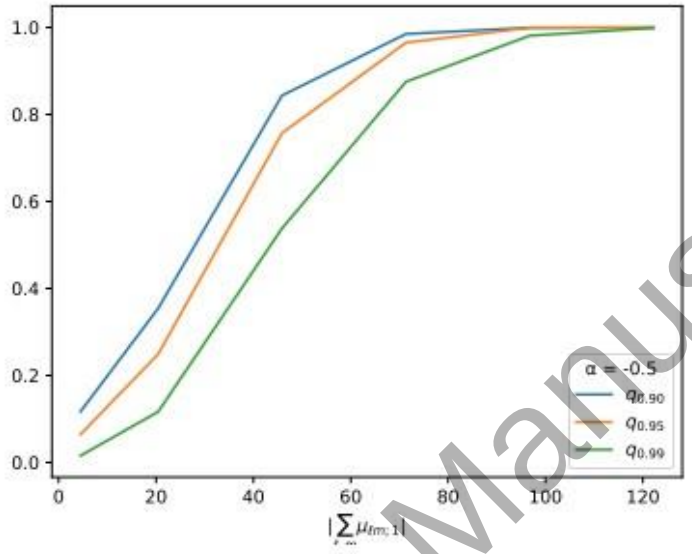

Figure 7: Left: test's power under the *deterministic trend* scenario for $\alpha = 0.2$, computed for $L = 10$, bandwidth $k_N = 5 \cdot [N^{1/3}]$, and based on 2000 independent replicates. Right: test's power under the *nontrivial power alternative* scenario, computed for $L = 10$, $N = 100$, bandwidth $k_N = 5 \cdot [N^{1/3}] = 20$, and based on 2000 independent replicates. The lines correspond to the selected quantiles of order 0.90 (blu line), 0.95 (orange line), 0.99 (green line).

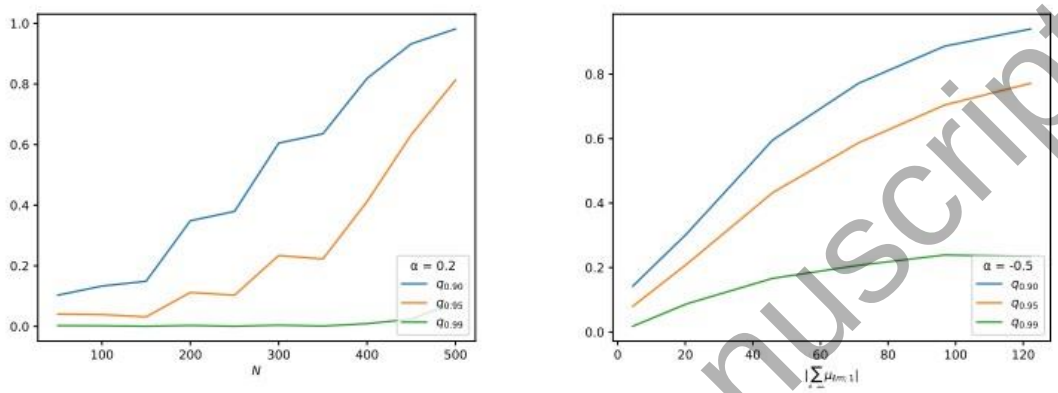

Figure 8: *Global surface temperature anomalies data*: observed CUSUM test statistic (2.4) computed over the window of consecutive multipoles $\{0,1,\ldots,12\}$, and bandwidth $k_N = [N^{1/3}] = 4$.

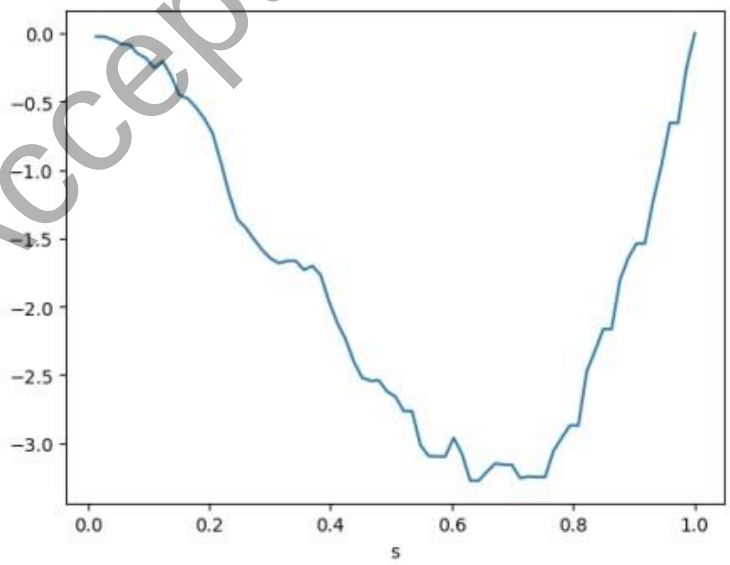

Table 1: Type I error probability corresponding to the selected quantiles of order $1-\gamma = 0.90, 0.95, 0.99$, computed for $L = 20$, bandwidth $k_N = [N^{1/3}]$, and based on 2000 independent replicates.

N	$q_{0.90}$	$q_{0.95}$	$q_{0.99}$
50	0.1	0.0555	0.0135
100	0.0955	0.047	0.0095
200	0.105	0.05	0.0115

Table 2: *Global surface temperature anomalies data*: observed CUSUM test statistic (2.4) computed over the window of consecutive multipoles $\{\underline{\ell}, \underline{\ell}+1, \ldots, 12\}$. Approximate *p*-values are based on 10^6 independent replicates of a Brownian bridge, each evaluated on a grid of 10^6 equally-spaced points over the unit interval.

$\underline{\ell}$	**0**	**1**	**2**	**4**	**6**	**8**
sup	3.27	2.94	2.72	2.17	1.83	1.48
p-value	< 0.0001	< 0.0001	< 0.0001	0.00011	0.00247	0.02509